Hindawi
Science and Technology of Nuclear Installations
Volume 2019, Article ID 4081943, 16 pages
https://doi.org/10.1155/2019/4081943

Research Article

Validation of Modified ART Mod 2 Code through Comparison with Aerosol Deposition of Cesium Compound in Phébus FPT3 Containment Vessel

Wasin Vechgama,[1] **Kampanart Silva**,[1] **and Somboon Rassame**[2]

[1]*Thailand Institute of Nuclear Technology (Public Organization), 9/9 Moo 7, Saimoon, Ongkharak, Nakhon Nayok, 26120, Thailand*
[2]*Department of Nuclear Engineering, Faculty of Engineering, Chulalongkorn University, 254 Phayathai Rd., Pathumwan, Bangkok, 10330, Thailand*

Correspondence should be addressed to Wasin Vechgama; wasinvechgama@gmail.com

Received 3 August 2018; Revised 17 December 2018; Accepted 31 December 2018; Published 3 February 2019

Guest Editor: Gonzalo Jimenez

Evaluation of aerosol deposition in the containment vessel is an important step for the assessment of radioactive material release to the environment. ART Mod 2 is a calculation code that is used for evaluation of aerosol deposition in the containment vessel. The authors modified aerosol deposition models of ART Mod 2, namely, gravitational settling model, Brownian diffusion model, diffusiophoresis model, and thermophoresis model in order to increase potential of capturing the deposition phenomena. This study aims to compare the simulated results of modified ART Mod 2 with aerosol deposition of cesium compounds in the containment vessel of Phébus FPT3 experiment, in order to validate modified ART Mod 2 code. It is found that aerosol deposition using modified ART Mod 2 agrees with Phébus FPT3. Prediction of Brownian diffusion is significantly improved due to the consideration of turbulent damping process. Cesium mass flow rate and aerosol size are factors that can significantly influence the uncertainty of the results. When conditions of single volumes are carefully selected to match those of the Phébus FPT3 experiment, modified ART Mod 2 can predict aerosol deposition in Phébus FPT3 with relative accuracy.

1. Introduction

Thailand Institute of Nuclear Technology (TINT) and Chulalongkorn University (CU) have been conducting research on nuclear power plant safety since 2012, putting emphasis on severe accident studies. The reason to this is that the Fukushima Accident, which is a severe accident, has driven attention of the public toward nuclear power safety, and thus it is the appropriate place to start. Currently, there are four main research topics, aiming to grasp the overview of the severe accident. The first research topic [1] is on thermal hydraulic assessment in reactor coolant system using SCDAP/RELAP5 of Innovative Systems Software (ISS), which aims to understand the situation of the reactor cooling system (RCS) during severe accidents. The second research topic is on assessment of cesium compound behavior in containment vessel using ART Mod 2 of Japan Atomic Energy Research Institute (JAERI), which aims to understand the behavior of cesium compounds in containment vessel (this study). The third research topic [2] is on the experiment of cesium compound behavior under high pressure and high temperature conditions, which aims to understand the behavior of cesium compound from experiment. The last research topic [3, 4] is on the consideration of accident consequence assessment methodology which can cover the overall consequences for people and the environment, in order to be able to consider consequences other than health effects due to radiation exposure which was basically the only thing considered in preceding studies.

Assessment of fission product behavior in containment vessel, the second topic, is important to understand the whole sequence of a severe accident. It is used to link two assessments together: (1) assessment of fission product behavior in reactor core and (2) assessment of consequences of fission product on people and environment. This study was thus launched in Thailand in order to evaluate and

collect essential data of fission product behavior, especially cesium compounds. There are a number of widely used computer programs for fission product behavior evaluation, such as MELCOR 2.1 [9] and CONTAIN 2.0 [10] of United States Nuclear Regulatory Commission, ASTEC 2.1 and SOPHAEROS 2.2 [11] of Institut de Radioprotection et de Sûreté Nucléaire (IRSN), COCOSYS 1.2 [12] of Gesellschaft für Anlagen- und Reaktorsicherheit (GRS), and ART Mod 2 [13] of Japan Atomic Energy Research Institute (JAERI). ART Mod 2 code was developed by JAERI and had been actively updated until 1997 [14]. However, due to some reasons, JAERI stopped further updates and shared the source code to the Radiation Safety Information Computational Center (RSICC). Therefore, ART Mod 2 code is a good choice for a newcomer country like Thailand which is in its beginning stage of research and development in fission product behavior in containment vessel and would like to have access to the source code in order to further develop by itself. JAEA (previously JAERI) decided to resume the development in 2015 [14] after the Fukushima Accident, which makes it even more attractive for a newcomer country since the code can do more with the updated version. In the latest validation work of ART Mod 2 by A. Hidaka et al. [15], gravitational settling and diffusiophoresis models of ART Mod 2 were validated using the NSPP-501, NSPP-502, NSPP-503, NSPP-504, and NSPP-505 experiments which studied the behavior of iron (III) oxide (Fe_2O_3) aerosols in saturated steam-air environment. As a result, there is good agreement between ART Mod 2 prediction and measured aerosol deposition. Additionally, in January 2015, ART Mod 2 was modified to correct coding errors and improve the vibration in the results of vapor calculation [14]. The latest ART Mod 2 is used to investigate the behavior of cesium iodide aerosols during containment bypass (BYP) in our previous study in which the deposition of cesium compound aerosols on the floor was largely overestimated [16]. Therefore, the authors started the research to modify and develop the aerosol deposition models of ART Mod 2 [17].

There have been several researches on comparison and validation of these computer codes with experiments, including Phébus FPT and ABCOVE & LACE experiments. For example, L. Herranz et al. [5] validated CONTAIN 2.0 using Phébus FPT1 experiment and J. Souto et al. [18] did the validation of MELCOR 1.8.2 code using ABCOVE & LACE experiments. G. Gyenes et al. [19] validated the CPA module (Containment Package implemented in the European integral code ASTEC) using Phébus FPT0, FPT1, and FPT2 experiments. L. Herranz et al. [20] validated several computer codes including CONTAIN 2.0, MELCOR 1.8.5, and ASTEC 1.1 using Phébus FPT0 and FPT1 experiments. Lastly, A. Kontautas et al. [21] validated COCOSYS using Phébus FPT2 experiment. It can be seen here that Phébus FPT and ABCOVE & LACE experiments are widely used for the validation of computer codes since they are integral tests which enable simultaneous evaluation of different aerosol deposition phenomena [22, 23]. In addition, all aerosol deposition phenomena match well with the aerosol deposition models of ART Mod 2, including gravitational settling, Brownian diffusion, diffusiophoresis, and thermophoresis; thus the authors selected the Phébus FPT experiments for the code validation in this study.

The authors focus on the evaluation of cesium compound behaviors since cesium (Cs) is one of the important aerosols of fission products that are released when nuclear fuels are overheated as in Phébus FPT3 experiment [6]. Phébus FPT3 experiment studied the effects of degradation of boron carbide (B_4C) control rod and fuel at 24.5 GWd/tU with steam-poor environment [6]. Volatile fission products from fuel are released into containment vessel in the forms of gas and aerosols. Iodine (I) and cesium (Cs) are dominant fission products in containment vessel [6]. Various cesium compounds including cesium iodine (CsI), cesium hydroxide (CsOH), and cesium molybdate (Cs_2MoO_4) are assumed to be released from the reactor core and have been actively investigated [6, 7, 24, 25]. CsI can be obtained when the released Cs reacts promptly with I. CsOH occurs when the amount of released cesium excesses that of iodine [24]. Though it has been traditionally assumed that all excess cesium will form CsOH, Phébus experiments show that cesium probably reacts with molybdenum (Mo) forming Cs_2MoO_4 [24]. Yet from some fission product studies, a chemical equilibrium between CsOH and Cs_2MoO_4 was found in the containment vessel [7, 26]. In this research, only aerosols of CsOH are selected for the validation of the modified ART Mod 2 with Phébus FPT3 experiment because there are less chances for CsI to be generated due to the presence of 80% of gaseous iodine in the containment vessel of Phébus FPT3 experiment [6]. Additionally, CsOH can represent Cs_2MoO_4 since they are at the chemical equilibrium in the containment vessel [7, 26].

Based on reasons mentioned above, the objective of this paper is to validate modified ART Mod 2 by comparing the simulated results of aerosol deposition of CsOH in the containment vessel with experimental results of Phébus FPT3 in order to confirm the ability of the code to evaluate the aerosol deposition of cesium compound in containment vessel. The paper is divided into five sections. This section introduces the background and the objective of the study. The second section explains Phébus FPT3 experiment. The third section describes the aerosol deposition models in ART Mod 2 code and modification of aerosol deposition models. The fourth section contains the calculation conditions for the comparison of the simulated results of modified ART Mod 2 with experiments, and the results and discussion. The last section is the conclusions.

2. Phébus FPT3 Experiment

Phébus FPT experiments of Institut de Radioprotection et de Sûreté Nucléaire (IRSN) started in 1988 to study strategies for reactor core meltdown accidents and determine the radioactive releases to the environment [25]. The latter includes the study on fission product behavior in Phébus FPT containment vessel, which is the main focus of this research. There were five experiments in the plan of Phébus FPT experiments. Table 1 [5, 22] shows a brief description of each experiment which has different types of flow, fuel, and sump conditions.

Table 1: Phébus FPT matrix [5, 22].

Phébus FPT matrix	Date	Flow	Fuel	Containment
FPT0	2/12/1993	Steam rich (Oxidizing)	Fresh irradiated 9 d. + Ag-In-Cd Control rod	Acidic sump 90°C pH 5
FPT1	26/07/1996	Steam rich (oxidizing)	BR3 23 GWd/tU + Ag-In-Cd Control rod	Acidic sump 90°C pH 5
FPT2	12/10/2000	Steam poor (steam starvation) + Boric acid	BR3 32 GWd/tU + Ag-In-Cd Control rod	Evaporating alkaline sump 90°C then 120°C pH 9
FPT3	18/11/2004	Steam poor (steam starvation)	BR3 23 GWd/tU B_4C Control rod	Evaporating alkaline sump 90°C then 120°C pH 5 + Recombiners
FPT4	22/07/1999	Debris Bed Steam + H_2 (low volatile & actinides release)	Gravelines 38 GWd/tU + Oxidised cladding Shards	-

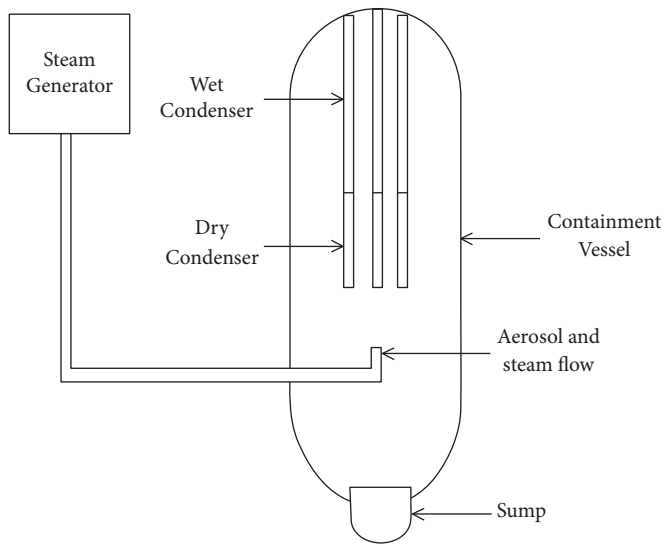

Figure 1: Geometry of Phébus FPT containment vessel [5].

Figure 1 shows the geometry of Phébus FPT containment vessel [5]. The 10 m^3 containment volume is divided into vertical wall, elliptic roof, elliptic bottom, and sump wall. There are three condensers inside the containment vessel. Each condenser is divided into the following: dry part condenser or hot part condenser, and wet part condenser or cold part condenser. Design parameters of each Phébus FPT experiment are shown in Table 2 [5].

Phébus FPT3 experiment studied the effects of degradation of boron carbide (B_4C) control rod and fuel, and the behaviors of gaseous iodine and cesium aerosols in the containment vessel [6]. Phébus FPT3 experiment [25] starts the transient from degradation phase which lasts about 5-6 hours. There is oxidation of fuels and control rods under steam-poor environment. Then the transient continues to the aerosol phase which takes place for about 37 hours. Aerosol transportation and deposition are studied in this phase. Next is the 23-minute-washing phase where aerosols are washed off toward the sump. The last phase is the chemistry phase where chemistry in containment and sump under severe accident conditions is analyzed. Thermal hydraulic conditions in the containment vessel of degradation phase, aerosol phase, washing phase, and chemistry phase are shown in Tables 3–6, respectively.

Table 2: Design parameters of the Phébus FPT experiment [5].

Structure	Type	Diameter [m]	Height [m]	Area [m^2]
		Vessels		
Wall	Cylinder	1.77	3.306	18.38
Roof	Slab	1.76	0.613	3.866
Floor	Slab	1.76	0.533	3.384
		Condensers		
Wet part	Cylinder	0.15	1.645	0.775
Dry part	Cylinder	0.15	0.713	0.336
		Sump		
Collar	Cylinder	0.584	0.108	0.2

Table 3: Thermal hydraulic conditions of the degradation phase [25].

Thermal hydraulic conditions	Phébus FPT3 experiment
Steam flow rates [g/s]	0.5
Sump temperature [K]	363
Containment gas temperature [K]	383
Condenser wet part temperature [K]	363
Condenser dry part temperature [K]	393
Containment pressure [bar]	2.1

Table 4: Thermal hydraulic conditions of the aerosol phase [25].

Thermal hydraulic conditions	Phébus FPT3 experiment
Sump temperature [K]	363
Containment gas temperature [K]	381
Condenser wet part temperature [K]	363
Condenser dry part temperature [K]	393
Containment pressure [bar]	2.0

Table 5: Initial thermal hydraulic conditions of the washing phase [25].

Initial thermal hydraulic conditions	Phébus FPT3 experiment
Sump temperature [K]	343
Containment gas temperature [K]	383
Condenser wet part temperature [K]	343
Condenser dry part temperature [K]	393
Containment pressure [bar]	1.6

Table 6: Mean thermal hydraulic conditions of the chemistry phase [25].

Mean thermal hydraulic conditions	Phébus FPT3 experiment
Sump temperature [K]	373
Containment gas temperature [K]	376
Condenser wet part temperature [K]	338
Condenser dry part temperature [K]	383
Containment pressure [bar]	1.7

Table 7: Characteristics of the Cs aerosol population in the containment vessel of Phébus FPT3 experiment [6].

Sampling time [s]	FPT3 phase	AMMD [μm]	GSD
10687	Degradation phase	0.81	2.1
11894	Degradation phase	1.45	2.7
19074	Cooling phase (part of degradation phase)	3.09	1.5
22648	Beginning of aerosol phase	3.35	1.5

Figure 2 shows the inlet Cs mass flow rate from the steam generator through a small pipe to the containment vessel measured with online gamma spectrometry [6]. Table 7 shows Aerodynamic Mass Median Diameter (AMMD) and Geometric Standard Deviation (GSD) of Cs aerosols [6]. Note that there are also other types of aerosols being released to the containment vessel though they are out of the scope of this study.

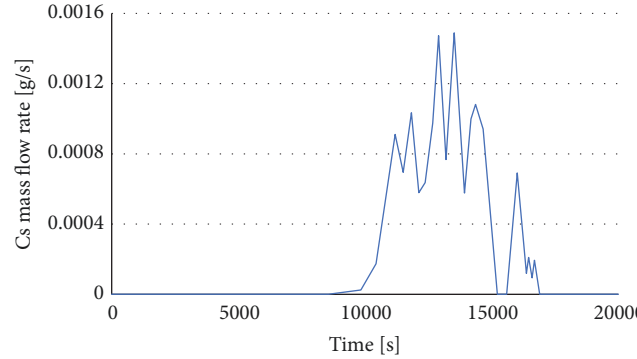

Figure 2: Cs mass flow rate to containment vessel in Phébus FPT3 experiment measured with online gamma spectrometry [6].

3. Models of ART Mod 2 Code

3.1. General Aerosol Transportation and Deposition in ART Mod 2. Figure 3 shows the calculation flow of ART Mod 2 which adopts implicit method; i.e., values of source term are updated within every time step. There are two main processes affecting the aerosol behavior, namely, transportation and deposition [13].

The calculation starts with the evaluation of the aerosol transportation among phases and among volumes. The governing equation for transportation by fluid calculates single-phase and multiphase aerosol transportation and aerosol removal as follows:

$$\begin{aligned}\left(\frac{dM_{p,I}^{k}(t)}{dt}\right)_{Transport\ by\ fluid} &= \sum_{J=1}^{N}\left(\frac{G_{J,I}^{gg}}{V_{g,I}}+\frac{G_{J,I}^{lg}}{V_{g,I}}\right)M_{p,I}^{k}(t) \\ &+ \sum_{j=1}^{N}\left[1-F_{pI,J}(t)\right]\frac{G_{I,J}^{gg}}{V_{g,I}}M_{p,I}^{k}(t) \\ &+ \sum_{j=1}^{N}\left[1-E_{sc\,I,J}(r_P,t)\right]\frac{G_{I,J}^{lg}}{V_{g.J}}M_{p,I}^{k}(t),\end{aligned} \tag{1}$$

where

$(dM_{p,I}^{k}(t)/dt)_{Transport\ by\ fluid}$ is the mass transfer rate to floor of radionuclide k in the p section at volume I [g/s],

$M_{p,I}^{k}$ is the mass of radionuclide k in the p section at volume I [g],

$G_{J,I}^{gg}$ is the gas to gas flow rate of the bulk fluid from the volume I to J [cm^3/s],

$G_{I,J}^{gg}$ is the gas to gas flow rate of the bulk fluid from the volume J to I [cm^3/s],

$G_{J,I}^{lg}$ is the liquid to gas flow rate of the bulk fluid from the volume I to J [cm^3/s],

$G_{I,J}^{lg}$ is the liquid to gas flow rate of the bulk fluid from the volume J to I [cm^3/s],

$F_{pI,J}(t)$ is the aerosol removal efficiency of the filter in the p section [-],

$E_{sc\,I,J}(r_P,t)$ is the aerosol scrubbing efficiency in the p section [-],

$V_{g,I}$ is the volume of the gas phase in the volume I, [cm^3],

$V_{g,J}$ is the volume of the gas phase in the volume J, [cm^3].

On the right hand side of (1), the first term shows single-phase and multiphase aerosol transportation between two volumes while the second and third terms show aerosol removal from filter and scrubbing between two volumes, respectively. The transportation scheme is shown in Figure 4.

Then ART Mod 2 calculates aerosol deposition on wall and on floor. The governing equation used to explain aerosol deposition on wall and on floor is as follows:

$$\begin{aligned}\left(\frac{dM_{p,I}^{k}(t)}{dt}\right)_{Deposition} &= -v_{d,I}(r_p)\frac{A_{w,I}}{V_{g,I}}M_{p,I}^{k}(t) \\ &- v_{dG,I}(r_p)\frac{A_{f,I}}{V_{g,I}}M_{p,I}^{k}(t),\end{aligned} \tag{2}$$

where

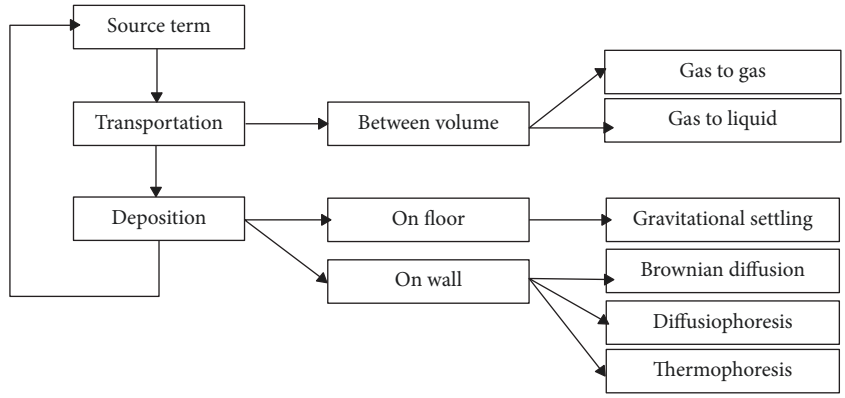

Figure 3: Calculation flow of ART Mod 2.

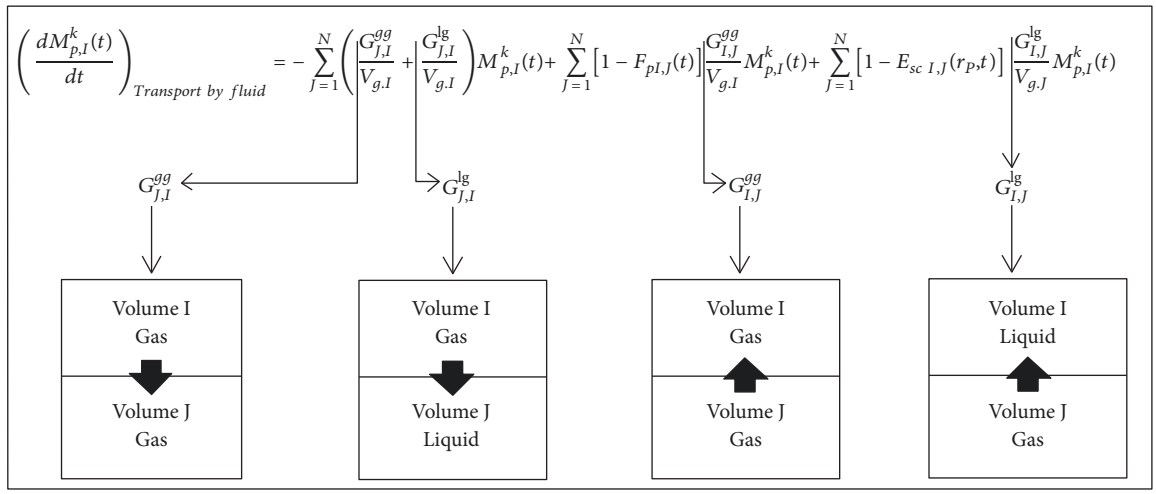

Figure 4: Aerosol transportation calculation scheme of ART Mod 2.

$(dM^k_{p,I}(t)/dt)_{Transport\ by\ fluid}$ is the mass transfer rate to wall of the radionuclide k in the p section at the volume I [g/s],

$M^k_{p,I}$ is the mass of radionuclide k in the p section at volume I [g],

$A_{w,I}$ is the deposition area of the structure surface at the volume I [cm^2],

$A_{f,I}$ is the deposition area of the floor or liquid surface at the volume I [cm^2],

$v_{d,I}(r_p)$ is the deposition velocity of the aerosol in the p section [cm/s],

$v_{dG,I}(r_p)$ is the deposition velocity of the aerosol by gravitational settling in the p section [cm/s].

On the right hand side of (2), the first term calculates aerosol deposition on wall while the second term shows aerosol deposition on floor. $v_{d,I}(r_p)$ and $v_{dG,I}(r_p)$ represent aerosol deposition velocities on wall and on floor, respectively. There are three phenomena determining the aerosol deposition on wall, namely, Brownian diffusion, diffusiophoresis, and thermophoresis, while aerosol deposition on floor is entirely due to the gravitational settling. Therefore, (2) can be rewritten as

$$\begin{aligned}\left(\frac{dM^k_{p,I}(t)}{dt}\right)_{Deposition} &= -v_{diff}(r)\frac{A_{w,I}}{V_{g,I}}M^k_{p,I}(t)\\ &\quad - v_{diffph}(r)\frac{A_{w,I}}{V_{g,I}}M^k_{p,I}(t)\\ &\quad - v_{ther}(r)\frac{A_{w,I}}{V_{g,I}}M^k_{p,I}(t)\\ &\quad - v_{gra}(r)\frac{A_{f,I}}{V_{g,I}}M^k_{p,I}(t).\end{aligned} \tag{3}$$

For aerosol deposition on wall, $v_{d,I}(r_p)$ represents aerosol deposition velocity due to Brownian diffusion ($v_{diff}(r)$) [cm/s], diffusiophoresis ($v_{diffph}(r)$) [cm/s], and thermophoresis ($v_{ther}(r)$) [cm/s]. For aerosol deposition on floor, $v_{dG,I}(r_p)$ represents aerosol deposition velocity due to gravitational settling ($v_{gra}(r)$) [cm/s].

3.1.1. Gravitational Settling. Aerosol deposition velocity due to gravitational settling, $v_{gra}(r)$, is derived from drag force of aerosol surface which varies with Reynolds number, Re, [-]. In the case of small Reynolds number (Re < 1), settling velocity of aerosols is calculated by the Stokes approximation. Otherwise settling velocity of aerosols is calculated by the Newton's approximation [13]:

$$v_{gra}(r) = \begin{cases} \dfrac{2r^2 g\left(\rho_p - \rho_g\right)}{9\mu_g} Cu(r), & \text{Re} < 1 \\ \dfrac{\mu_g \text{Re}}{2r\rho_p}, & \text{Re} > 1, \end{cases} \quad (4)$$

where

r is the radius of aerosol, [cm],

g is the gravitational acceleration, [cm/s^2],

ρ_p is the density of aerosol, [g/cm^3],

ρ_g is the density of gas, [g/cm^3],

$Cu(r)$ is the Cunningham factor, [-],

μ_g is the viscosity of gas, [dyn-s/cm^2].

Cunningham factor, $Cu(r)$, [-], is an empirical function of Knudsen number, Kn, [-], which helps taking into account the effect of particle slip:

$$Cu(r) = 1 + \text{Kn}\left[1.26 + 0.42\exp\left(\frac{-0.87}{\text{Kn}}\right)\right]. \quad (5)$$

Knudsen number, Kn, [-], can be calculated from mean free path, λ, [cm], and radius of aerosol, r, [cm]:

$$\text{Kn} = \frac{2\lambda}{r}. \quad (6)$$

The mean free path, λ, [cm], is derived from average gas molecular velocity [13]:

$$\lambda = \frac{k_B T_g}{4\pi a^2 \sqrt{2} P_t} \quad (7)$$

where

k_B is the Boltzmann constant, [J/K],

T_g is the temperature of gas, [K],

a is the radius of gas molecule, [cm],

P_t is the total pressure of gas, [MPa].

3.1.2. Brownian Diffusion. Aerosol deposition velocity due to Brownian diffusion, $v_{diff}(r)$, can be simply obtained from the Fick's law of diffusion [13]:

$$v_{diff}(r) = \frac{D_p(r)}{\delta_D}. \quad (8)$$

where

$D_p(r)$ is the aerosol diffusion coefficient, [cm^2/s],

δ_D is the thickness of boundary layer, δ_D [cm].

Aerosol diffusion coefficient, $D_p(r)$, [cm^2/s], is calculated using

$$D_p(r) = \frac{k_B T_g}{6\pi\mu_g r} Cu(r). \quad (9)$$

Thickness of boundary layer, δ_D [cm], is calculated by the empirical model obtained from the study of 0.1 μm aerosols diffusion onto wall [27]:

$$\delta_D = 0.46 D_p(r)^{0.21}. \quad (10)$$

3.1.3. Diffusiophoresis. Aerosol deposition velocity due to diffusiophoresis, $v_{diffph}(r)$, is controlled by the flow of the condensing steam and partial pressures of noncondensable gas near the structure surface. The model of diffusiophoresis considers both velocity of Stephan flow and gas momentum transfer [13]:

$$v_{diffph}(r) = \frac{\sqrt{m_s}}{\gamma_s\sqrt{m_s} + \gamma_a\sqrt{m_a}} U_c, \quad (11)$$

where

m_s is the molecule weight of steam, [g],

m_a is the molecule weight of noncondensible gas, [g],

γ_s is the mole fraction of steam, [-],

γ_a is the mole fraction of noncondensible gas, [-],

U_c is the velocity of condensing steam, [cm/s].

The velocity of condensing steam takes into consideration the Brownian limit and the convective diffusion limit:

$$\frac{1}{U_c} = \frac{1}{k_c} + \frac{1}{k_n}, \quad (12)$$

k_c is the velocity of the condensing steam inside the boundary layer [cm/s],

k_n is the velocity of steam by convective diffusion [cm/s].

The velocity of the condensing steam inside the boundary layer, k_c [cm/s], which represents the Brownian limit, and the velocity of steam by convective diffusion, k_n [cm/s], can be estimated by

$$k_c = \frac{D_{sa}}{1 - \gamma_s} \nabla\gamma_s, \quad (13)$$

where

$\nabla\gamma_s$ is the gradient of mole fraction of steam, [-],

$$k_n = \frac{D_{sa}}{L} \text{Sh}, \quad (14)$$

where

Sh is the Sherwood number, [-],

L is the length of deposition surface, [cm].

3.1.4. Thermophoresis. Aerosol deposition velocity of aerosols from thermophoresis, $v_{ther}(r)$, [cm/s], is affected by convective diffusion of aerosol in the case of large system, such as in actual power plants, as in the case of diffusiophoresis. Therefore,$v_{ther}(r)$ is the combination of the velocity of thermophoresis, $v_T(r)$, [cm/s], and the velocity of convective diffusion, $k_n(r)$, [cm/s] [13]:

$$v_{ther}(r) = \frac{v_T(r)\, k_n(r)}{v_T(r) + k_n(r)}. \tag{15}$$

The calculation of velocity of thermophoresis is divided into two cases according to the value of the Knudsen number from Block's model and Epstein's model, respectively:

$$v_T(r) = \begin{cases} \dfrac{3\nu_g Cu(r)\left(\lambda_g + C_t \mathrm{Kn}(r)\,\lambda_p\right)}{2T_g\left(1 + 3C_m \mathrm{Kn}(r)\right)\left(2\lambda_g + \lambda_p + 2C_t \mathrm{Kn}(r)\,\lambda_p\right)}\nabla T_g, & \mathrm{Kn} < 0.2 \\ \dfrac{3\nu_g}{4\left(1 + (\pi/8)\,\alpha_m\right)T_g}\nabla T_g \exp\left(\dfrac{-\left(0.09 + 0.12\alpha_m\right)\left(1 - \alpha_t\left(\lambda_g/2\lambda_p\right)\right)}{\mathrm{Kn}}\right), & \mathrm{Kn} > 0.2, \end{cases} \tag{16}$$

where

ν_g is the dynamic viscosity of gas, [cm^2/s],

λ_g is the conductivity of mixed gas, [erg/(K.cm.s)],

λ_p is the conductivity of aerosol, [erg/(K.cm.s)],

C_t is the coefficient of the energy exchanges between the aerosol and gas, [-],

C_m is the coefficient of the momentum exchanges between the aerosol and gas, [-],

α_m is the accommodation factor for momentum exchange, [-],

α_t is the accommodation factor for energy exchange, [-],

∇T_g is the gradient of temperature of gas, [K].

3.2. Modification of Aerosol Deposition Models in ART Mod 2

3.2.1. Gravitational Settling. It was found in the gravitational settling model of ART Mod 2 code that the applicable range of aerosol size was not identified for (5) though it can affect the particle slip [13]. In addition, when the average gas molecular velocity is used in the calculation of the mean free path, positive velocities can be offset by the negative ones which may lead to underestimation. Therefore, the authors replaced (5) with an equation derived from empirical model for the slip of spherical particles with a diameter less than 15 μm [8] which matches with the range of aerosol particle size in Phébus FPT3 [23]:

$$Cu(r) = 1 + \mathrm{Kn}\left[1.142 + 0.588\exp\left(\frac{-0.999}{\mathrm{Kn}}\right)\right]. \tag{17}$$

The root mean square velocity is used instead of the average velocity for the mean free path calculation to avoid the offset of velocities with different directions [28]:

$$\lambda = \frac{\mu_g}{\rho_g}\sqrt{\frac{M_w}{3k_B T}}. \tag{18}$$

Here

M_w is the molecular weight of gas, [g].

3.2.2. Brownian Diffusion. Fick's law of diffusion is used to evaluate deposition on wall in Brownian diffusion model in ART Mod 2 code. However, from previous researches [16, 17], it is found that Fick's law of diffusion may lead to underestimation of Brownian diffusion especially in the case of turbulent flow. Moreover, the size of aerosols used in the experiment deriving (12) does not match the aerosol sizes of the Phébus FPT experiments [23, 29]. Modified ART Mod 2 adopts an empirical model considering turbulent damping process under the conditions of upward flow direction in vertical duct, particle size around 2-4 μm, and volumetric flow rate around 0.00062-0.005 m^3/s [29] for the calculation of the aerosol deposition velocity due to Brownian diffusion. It is a function of the dimensionless particle relaxation time, τ^+, Schmidt number, Sc, and friction velocity, u_τ [30].

$$v_{diff} = \begin{cases} 0.0899\mathrm{Sc}^{-0.704}u_\tau; & \tau^+ < 0.2 \\ 3.25\times 10^{-4}\tau^{+2}u_\tau; & 0.2 < \tau^+ < 22.9 \\ 0.17u_\tau; & \tau^+ > 22.9 \end{cases} \tag{19}$$

The Schmidt number is calculated by

$$\mathrm{Sc} = \frac{\nu}{D_p(r)} \tag{20}$$

where

ν is the kinematic viscosity of fluid, [m^2/s].

The dimensionless particle relaxation time is calculated by

$$\tau^+ = \frac{\rho_p 4r^2}{18\mu_g^2}u_\tau^2\rho_g. \tag{21}$$

The friction velocity can be calculated from an equation known as the law of the wall, and it is found to satisfactorily correlate with experimental data for smooth surfaces [30]:

$$0 \le \frac{\delta_D u_\tau}{\nu} \le 5. \tag{22}$$

Table 8: Design conditions of containment vessel, dry condenser, and wet condenser in ART Mod 2.

Design conditions	Containment vessel volume	Dry condenser part volume	Wet condenser part volume
Diameter [m]	1.77	0.90	0.90
Height [m]	4.07	0.71	1.64
Total Area [m^2]	27.52	1.01	2.32
Total Volume [m^3]	10	2.01	4.65

3.2.3. Diffusiophoresis. For diffusiophoresis model in ART Mod 2 code, since the turbulent flow at high Reynolds and Knudsen numbers, as found in the Phébus FPT experiments, affects slip of particle [31], the modified ART Mod 2 introduces the Cunningham factor in (23) to account for this effect:

$$v_{diffph}(r) = \left[U_c + \frac{Cu(r)}{\chi} \frac{\sqrt{m_s}}{\gamma_s \sqrt{m_s} + \gamma_a \sqrt{m_a}} \gamma_a U_c\right]. \quad (23)$$

The new equation [31] also includes shape factor, χ [-], which affects the deposition of nonspherical particles [32]. However, as the particles in this study are assumed spherical, the shape factor is set to 1 and thus has no effect on the results.

3.2.4. Thermophoresis. For thermophoresis model in ART Mod 2 code, it is found that the two cases in (16) are empirically derived from difference experiments. Block's model calculates $v_T(r)$ at low conductivity and low Knudsen number, while Epstein's model is applied at high conductivity and high Knudsen number. However, there is a new model created by Monte-Carlo type numerical modeling which collapsed the two cases into a single equation to reduce complicacy in calculation [33]:

$$v_T(r) = \frac{2v_g Cu(r)\left(\lambda_g + C_t \mathrm{Kn}(r)\lambda_p\right)(1 + 9\mathrm{Kn}/(4 + \pi/2))}{T_g\left(1 + 3C_m \mathrm{Kn}(r)\right)\left(2\lambda_g + \lambda_p + 2C_t \mathrm{Kn}(r)\lambda_p\right)} \cdot \nabla T_g. \quad (24)$$

4. Comparison of the Simulated Results of Modified ART Mod 2 with Phébus FPT3 Experiment

4.1. Boundary Conditions. Temperatures, pressures, steam flow rates, source term, and aerosol size are important boundary conditions for ART Mod 2 code since they determine the aerosol deposition characteristics. Apart from the aerosol phase, the degradation phase also plays an important role in determining the physical properties of the aerosols. Therefore, the thermal hydraulics of both phases are used for the simulation.

In our previous study [16], the authors attempted to divide the containment vessel into multiple volumes in order to account for three-dimensional characteristics, e.g., circular flow. However, this could not be handled by ART Mod 2 code which is a one-dimensional code, resulting in large underestimation of the steam flow rates among volumes.

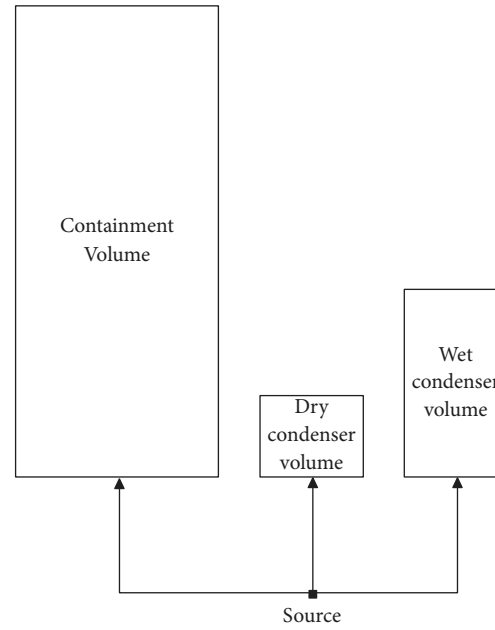

Figure 5: Nodalization of containment vessel, dry condenser, and wet condenser of Phébus FPT3 experiment in ART Mod 2.

On the other hand, A. Hidaka et al. [15] used ART Mod 2 to simulate the NSPP-501, NSPP-502, NSPP-503, NSPP-504, and NSPP-505 experiments using single volume to study the behavior of Fe_2O_3 aerosols in saturated steam-air environment and found that the deposition results agree with the NSPP experiments. Therefore, the author adopts the single volume approach in this study. Three different single volumes are used to represent the containment vessel, dry condenser, and wet condenser. The source is distributed to each volume based on the steam flow rate (see the details below). Figure 5 shows the nodalization and Table 8 shows the design conditions of each volume.

In degradation phase, gas temperature and pressure of all volumes are 383 K and 2.1 bars, respectively. Wall temperature of containment vessel is assumed to be equal to gas temperature because there is double-walled insulated tank to maintain temperature [23]. Temperatures of wet condenser and dry condenser volumes are maintained at 363 K and 393 K, respectively. Steam flow rate of the Phébus FPT3 experiment is constantly flown to containment vessel at 0.5 g/s [6]. However, there is oxidation reaction of fuel and steam, from which there are generation of hydrogen gas and consumption of steam using mole ratio at 1:1 [5]. Figures 6 and 7 show mass flow rate of hydrogen gas and steam, and volume fractions of hydrogen gas and steam, respectively. In

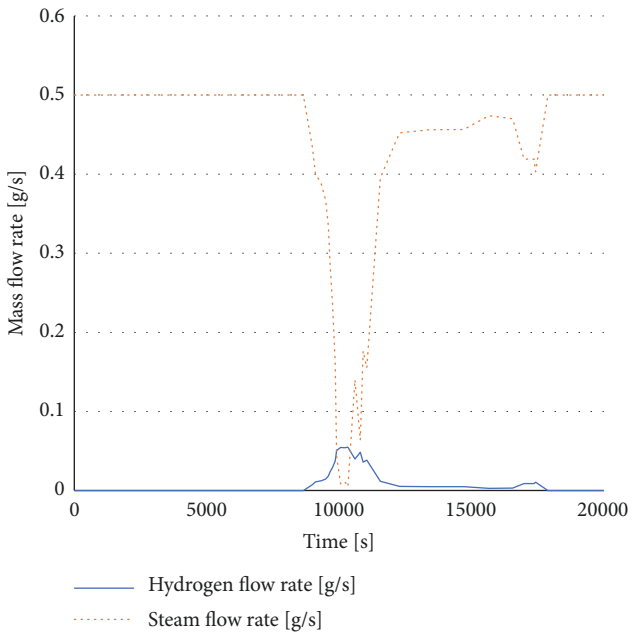

Figure 6: Mass flow rate of hydrogen gas and steam in ART Mod 2.

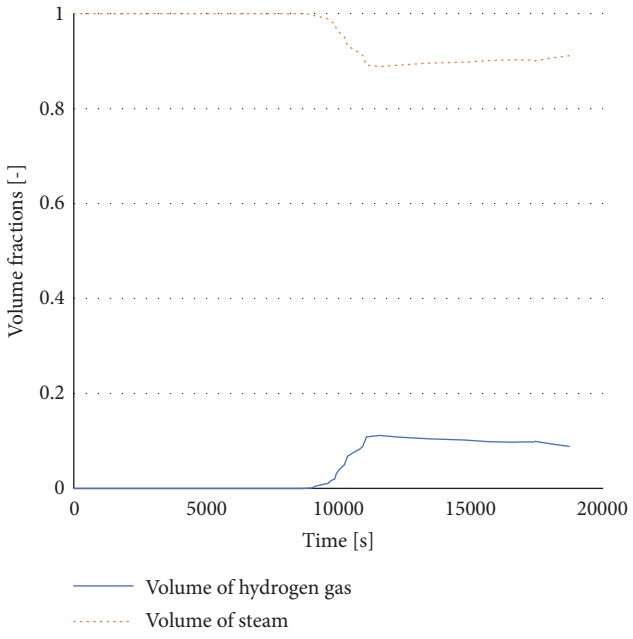

Figure 7: Volume fractions of hydrogen gas and steam in ART Mod 2.

the aerosol phase, reactor was shut down. Gas temperature and pressure in containment vessel reduce to 381 K and 2.0 bar, respectively.

Aerosol of CsOH is selected to represent behavior of cesium compounds. Distribution of CsOH mass flow rates to each single volume are estimated based on the fraction of the steam flow rates of each volume which were calculated by RELAP5 Mod 3.3 [34]. Nodalization of containment vessel of Phébus FPT3 experiment in RELAP5 Mod 3.3 is shown in Figure 8. The containment vessel is divided into three zone:

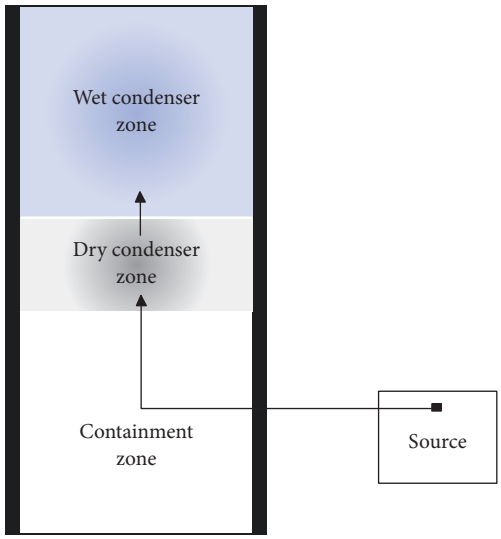

Figure 8: Nodalization of containment vessel of Phébus FPT3 experiment in RELAP5 Mod 3.3.

containment zone, dry condenser zone, and wet condenser zone. Design conditions are shown in Table 9. Temperature and pressure in the containment vessel are set at 383 K and 2.1 bar because the steam is fed in the degradation phase [25]. Wall temperature is set using heat slap at 383 K. Steam is flown into the containment vessel at the rate shown in Figure 6. Figure 9 shows steam flow rates of containment zone, dry condenser zone, and wet condenser zone derived from RELAP5 Mod 3.3 [34]. The fraction of the steam flow rate of each zone is multiplied by the Cs mass flow rate in Figure 2 to determine the CsOH mass flow rate of each volume in ART Mod 2 in Figure 5. Figure 10 shows CsOH mass flow rates into all volumes in ART Mod 2.

Values of AMMD and GSD of each phase in Table 7 are used to calculate the distribution of Cs compounds using log-normal approximation. These are used as input data for ART Mod 2 code. Table 10 shows the size distribution of Cs compounds from the degradation phase to the beginning of the aerosol phase.

4.2. Results and Discussion. The authors compare the results from modified ART Mod 2 with (1) the Phébus FPT3 experimental results measured with online gamma spectrometry in Table 11 [6, 23], (2) the Phébus FPT3 calculated results using deposition kinetic models in Figure 11 [6, 23], and (3) the results from original ART Mod 2 [13]. The simulation results of the three single volumes shown in Figure 5, namely, containment vessel volume, dry condenser volume, and wet condenser volume, are first described in sequence. Then the results of all volumes are combined based on CsOH mass flow rate fractions in Figure 10 to represent the situation in Phébus FPT3 experiment.

4.2.1. Containment Vessel Volume. Figures 12 and 13 show CsOH deposition in containment vessel volume calculated by ART Mod 2 and modified ART Mod 2, respectively. It is

Table 9: Design conditions of containment zone, dry condenser zone, and wet condenser zone in RELAP5 Mod 3.3.

Design conditions	Containment vessel zone	Dry condenser part zone	Wet condenser part zone
Diameter [m]	1.77	1.77	1.77
Height [m]	1.71	0.71	1.64
Total Area [m^2]	9.49	3.96	9.13
Total Volume [m^3]	4.20	1.76	4.04

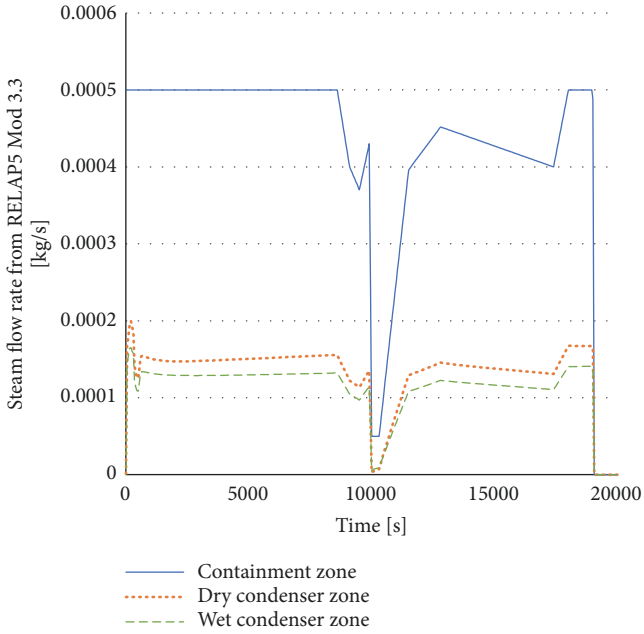

Figure 9: Steam flow rates of containment zone, dry condenser zone, and wet condenser zone from RELAP5 Mod 3.3.

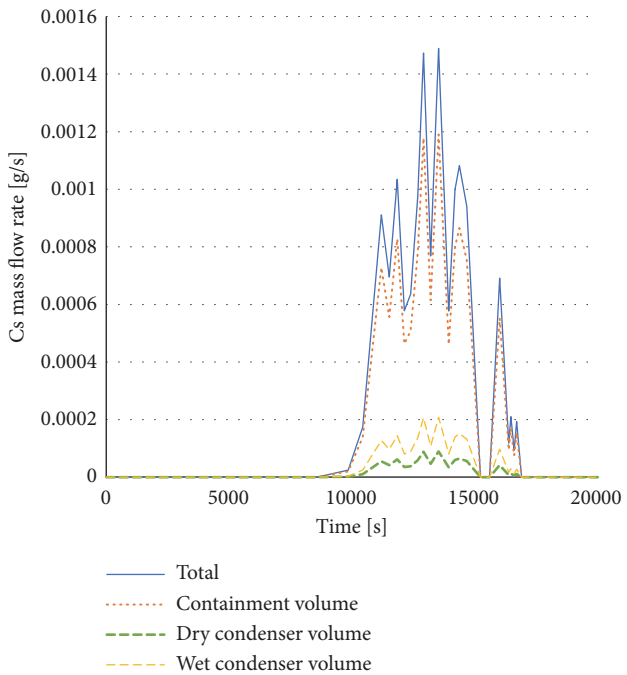

Figure 10: CsOH mass flow rates of containment volume, dry condenser volume, and wet condenser volume in ART Mod 2.

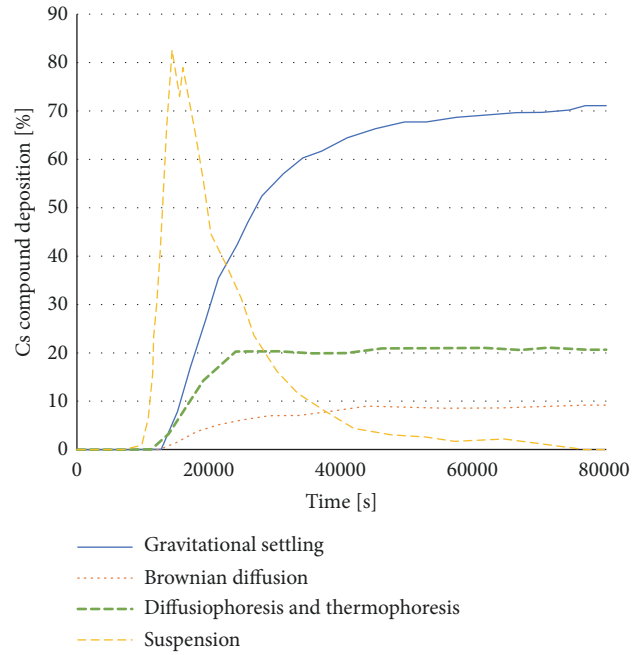

Figure 11: Phébus FPT3 calculated results using deposition kinetic models [7, 8].

found that most CsOH is deposited on containment floor due to gravitational settling [13]. Contribution of Brownian diffusion to the deposition on the containment wall after the modification of ART Mod 2 is in the same order as the experimental results in Table 11 and the calculated results using deposition kinetic models in Figure 11. Increase of Brownian diffusion after the modification of ART Mod 2 is attributed to the consideration of turbulent damping process. Equation (19) [29] divides the calculation into three cases depending on the dimensionless particle relaxation time, τ^+, [-]. When the Reynolds number is high, i.e., the flow is in the range of turbulent flow, the τ^+ is also high, thus (19) falls into the last case where Brownian diffusion significantly occurs. This is consistent with the findings in Haste et al. [23]. Diffusiophoresis and thermophoresis have negligible influence in the containment volume due to the inexistence of temperature gradient between the gas and the wall [17, 33].

4.2.2. Dry Condenser Volume. The simulation of dry condenser volume considers only aerosol deposition on wall because there is no floor on dry condenser. Figures 14 and 15 show CsOH deposition in dry condenser volume calculated by ART Mod 2 and modified ART Mod 2, respectively. Increase in Brownian diffusion after the code modification

Table 10: Size distribution of Cs compounds from the degradation phase to the beginning of the aerosol phase.

Time [s]	10687	11894	19074	22648
Phase	Degradation phase [μm]	Degradation phase [μm]	Cooling phase (part of degradation phase) [μm]	Beginning of aerosol phase [μm]
Percentile 5	2.39E-01	2.83E-01	1.59E+00	1.72E+00
Percentile 15	3.75E-01	5.18E-01	2.03E+00	2.20E+00
Percentile 25	4.91E-01	7.42E-01	2.35E+00	2.55E+00
Percentile 35	6.09E-01	9.89E-01	2.64E+00	2.87E+00
Percentile 45	7.38E-01	1.28E+00	2.94E+00	3.18E+00
Percentile 55	8.89E-01	1.64E+00	3.25E+00	3.53E+00
Percentile 65	1.08E+00	2.13E+00	3.61E+00	3.92E+00
Percentile 75	1.34E+00	2.83E+00	4.06E+00	4.40E+00
Percentile 85	1.75E+00	4.06E+00	4.70E+00	5.10E+00
Percentile 95	2.74E+00	7.43E+00	6.02E+00	6.53E+00

Table 11: Phébus FPT3 experimental results measured with online gamma spectrometry [6, 23].

Phenomenon	Deposition region	Deposition fraction [%]
Gravitational settling	On floor	58
Brownian diffusion	On wet condenser	8
Diffusiophoresis and thermophoresis	On wall and dry condenser	21

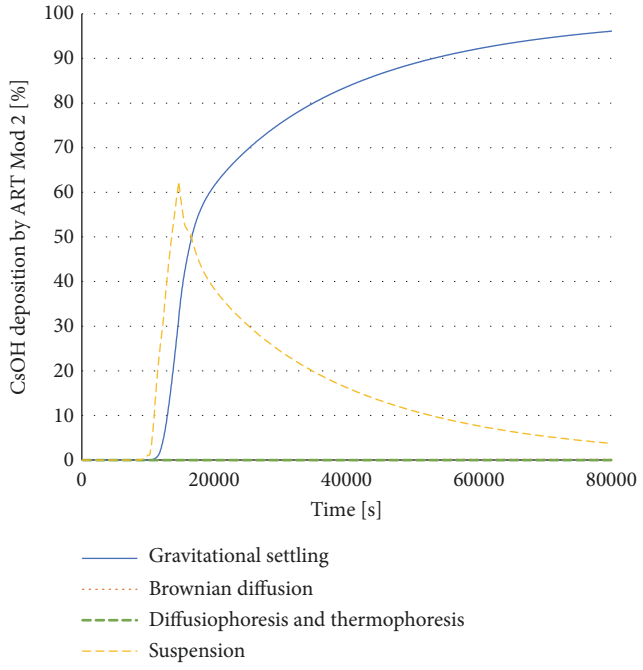

Figure 12: CsOH deposition in containment vessel volume calculated by ART Mod 2.

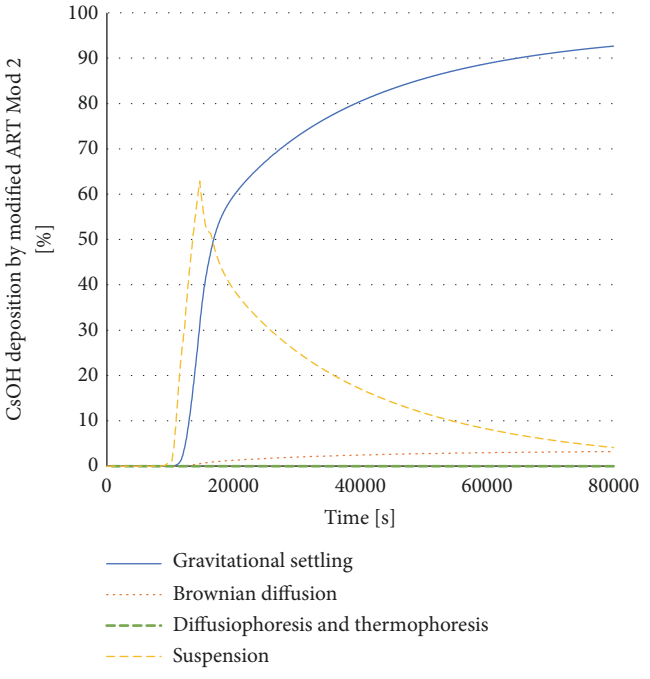

Figure 13: CsOH deposition in containment vessel volume calculated by modified ART Mod 2.

can be observed as in the case of containment volume. Diffusiophoresis and thermophoresis have negligible influence because the dry condenser wall temperature is higher than the gas temperature [17, 33].

4.2.3. Wet Condenser Volume. The simulation of wet condenser volume considers only aerosol deposition on wall because there is no floor on wet condenser. Figures 16 and 17 show CsOH deposition in wet condenser volume calculated by ART Mod 2 and modified ART Mod 2, respectively. It is found that most CsOH is deposited on wet condenser wall due to diffusiophoresis and thermophoresis both before and after the modification of ART Mod 2. These results

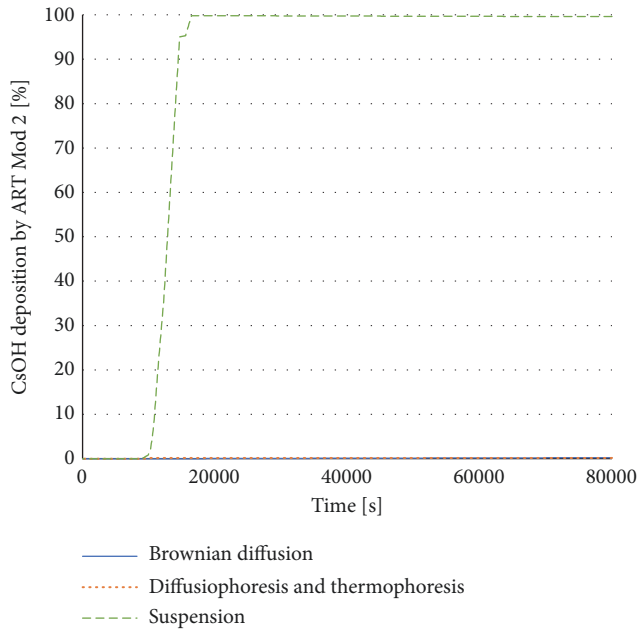

Figure 14: CsOH deposition in dry condenser volume calculated by ART Mod 2.

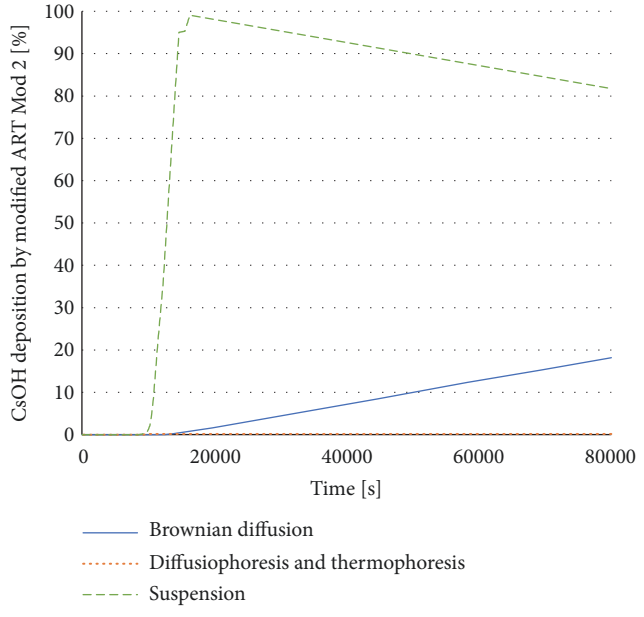

Figure 15: CsOH deposition in dry condenser volume calculated by modified ART Mod 2.

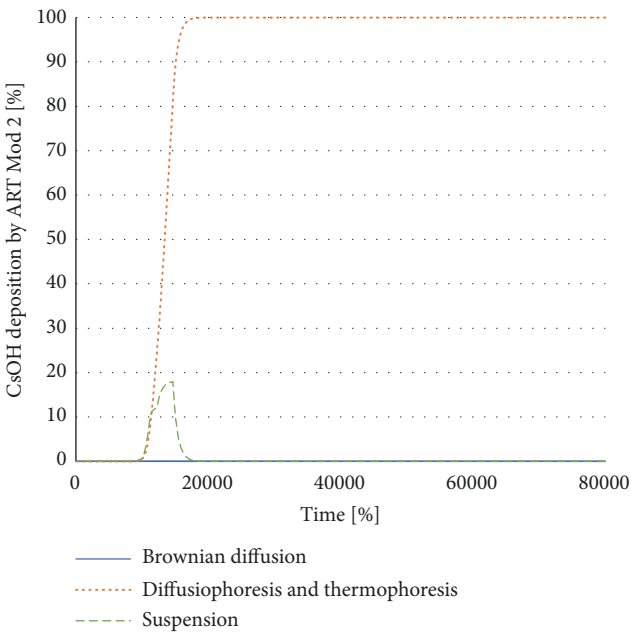

Figure 16: CsOH deposition in wet condenser volume calculated by ART Mod 2.

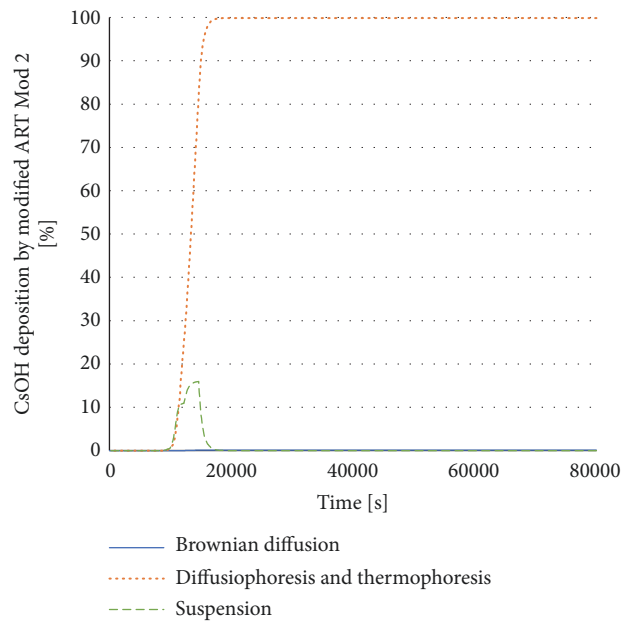

Figure 17: CsOH deposition in wet condenser volume calculated by modified ART Mod 2.

correspond to the experimental results in Table 11 and the calculated results in Figure 11. Diffusiophoresis occurs from the difference in partial pressure and momentum transfer of the system due to temperature difference between wet condenser wall and gas. Thermophoresis occurs because of the temperature gradient between wet condenser wall and gas. The two phenomena are considered identical in the Phébus FPT3 experiment. Diffusiophoresis is larger than thermophoresis by around 2 orders. Brownian diffusion is smaller than diffusiophoresis by around 3 orders because Brownian diffusion model is not sensitive with temperature difference between wet condenser wall and gas [13, 29].

4.2.4. Combination of All Volumes. Aerosol deposition in containment vessel, dry condenser, and wet condenser is combined based on the fraction of Cs mass flow rate in order to understand the whole system of containment vessel of the Phébus FPT3 experiment. Figures 18 and 19 show the CsOH deposition from the combination of calculation results of all

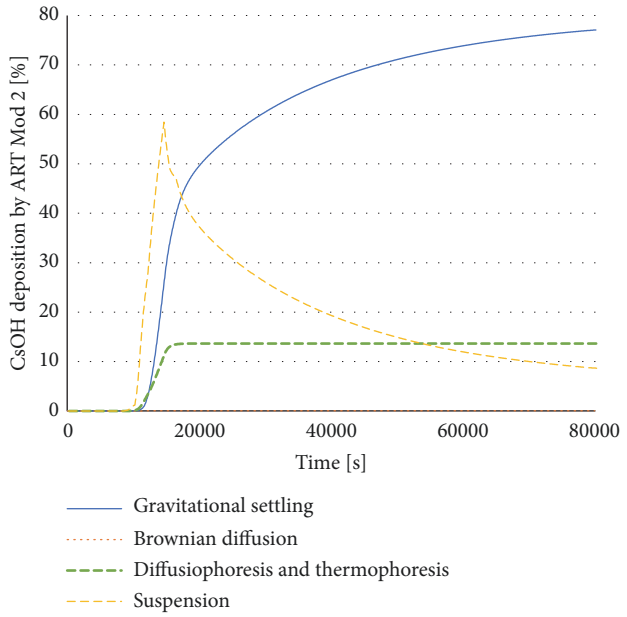

Figure 18: CsOH deposition from combination of calculations of all single volumes calculated by ART Mod 2.

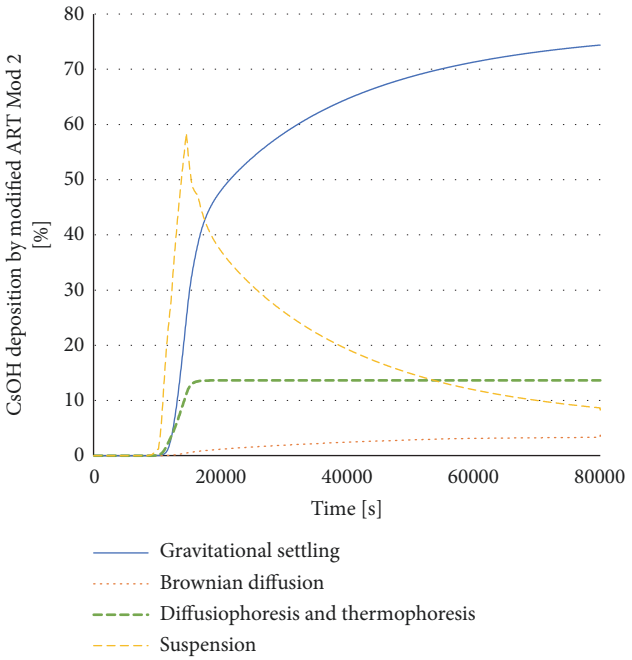

Figure 19: CsOH deposition from combination of calculations of all single volumes calculated by modified ART Mod 2.

single volumes calculated by ART Mod 2 and modified ART Mod 2, respectively.

After the modification of ART Mod 2, there is significant increase of Brownian diffusion on the wall of containment vessel and dry condenser. The values calculated by the modified ART Mod 2 are closer to those of the Phébus FPT3 experiment [6]. Diffusiophoresis (and thermophoresis) in wet condenser agree with the Phébus FPT3 experiment [23]. Most remaining CsOH is deposited on the floor of containment vessel from gravitational settling due to gravitational force and some remaining CsOH still suspends in containment vessel. This is again similar to the results of the Phébus FPT3 experiment in Table 11 [23].

However, it is found that there are slight underestimations of Brownian diffusion, diffusiophoresis, and thermophoresis and overestimation of gravitational settling when compared with the Phébus FPT3 experiment in Table 11 [23]. These may be attributed to the determination of CsOH mass flow rates of each single volume in ART Mod 2 which is assumed to follow the fractions of steam flow rate calculated by RELAP5 Mod 3.3. In the experiment, CsOH mass flow rates of each volume may change due to the circular flow which can only be considered in three-dimensional code [19]. This is one of the limitations of one-dimensional code [13]. Another source of uncertainties is the determination of distribution of aerosol size. The input was assumed to follow log-normal distribution which may be different from the distribution in the experiment. If the proportion of smaller aerosols is increased, the deposition on wall due to Brownian diffusion, diffusiophoresis, and thermophoresis will increase, deposition of gravitational settling will decrease [35], and vice versa. It can thus be concluded that the Cs mass flow rate and the aerosol size are the two main sources of uncertainties in the calculated results.

This study shows that ART Mod 2 code, even though it is a one-dimensional code, is appropriate for the simulation of Cs compound behavior in the containment vessel, since the aerosol deposition results calculated by the modified ART Mod 2 match well the Phébus FPT3 experiment. Another finding from the simulation is that single volume approach is more appropriate than the multiple volume approach for a one-dimensional code. This is supported by the study of A. Hidaka et al. where single volume is used to simulate the NSPP experiments in ART Mod 2 and resulted in a good agreement with the experiment [15]. Influence of circular flow has to be confirmed with a simulation in a three-dimensional code [19].

5. Conclusions

Aerosol deposition model of cesium compound in modified ART Mod 2 code was validated using Phébus FPT3 experiment.

(i) Aerosol deposition models of ART Mod 2, namely, gravitational settling, Brownian diffusion, diffusiophoresis, and thermophoresis, were modified considering appropriate boundary conditions and updates of deposition models.

(ii) Correlations of Cunningham factor and mean free path in the gravitational settling model were modified. Equation for the deposition velocity due to Brownian diffusion was modified to account for turbulent damping process. Cunningham factor was introduced to diffusiophoresis to consider particle slip. Thermophoresis model was modified to simplify the calculation scheme.

(iii) Contribution of Brownian diffusion to the deposition on the containment wall is in the same order as the Phébus FPT3 experiment. This is due to the consideration of turbulent damping process.

(iv) There are diffusiophoresis and thermophoresis on the wall of the wet condenser and gravitational settling on the floor of the containment which are the same as the Phébus FPT3 experimental results.

(v) Cs mass flow rate and the aerosol size are the two main sources of uncertainties in the calculated results.

(vi) Single volume approach is more appropriate than multiple volume approach for a simulation in a one-dimensional code.

Data Availability

The data used to support the findings of this study are available from the corresponding author upon request.

Conflicts of Interest

The authors declare that they have no conflicts of interest.

Acknowledgments

The authors would like to acknowledge Phébus FP consortium for the significant contribution of each developer in the build-up of the Phébus FP tests.

References

[1] N. Rattanadecho, S. Rassame, K. Silva et al., "Assessment of RELAP/SCDAPSIM/MOD3.4 prediction capability with severe fuel damage scoping test," *Science and Technology of Nuclear Installations*, vol. 2017, Article ID 7456380, 12 pages, 2017.

[2] K. Kanjana, "High-temperature setup for investigation of fission product behavior," in *Proceedings of the International Nuclear Science and Technology Conference*, Bangkok, Thailand, August 2016.

[3] K. Silva, Y. Ishiwatari, and S. Takahara, "Cost per severe accident as an index for severe accident consequence assessment and its applications," *Reliability Engineering & System Safety*, vol. 123, pp. 110–122, 2014.

[4] K. Silva and K. Okamoto, "A simple assessment scheme for severe accident consequences using release parameters," *Nuclear Engineering and Design*, vol. 305, pp. 688–696, 2016.

[5] L. E. Herranz, C. L. D. Prá, and A. M. Rincón, "CIEMAT contribution to the PHEBEN-2 project: interpretation of the PHEBUS-FPT1 experiment," *Informes Técnicos Ciema*, no. 1025, 2003.

[6] T. Haste, F. Payot, C. Manenc et al., "Phébus FPT3: Overview of main results concerning the behaviour of fission products and structural materials in the containment," *Nuclear Engineering and Design*, vol. 261, pp. 333–345, 2013.

[7] T.-M. Do, S. Sujatanond, Y. Tachibana, and T. Ogawa, "Vaporization and deposition of cesium dimolybdate, Cs2Mo2O7," *Journal of Nuclear Science and Technology*, vol. 54, no. 3, pp. 330–336, 2017.

[8] H. J. Allelein, A. Auvinen, J. Ball et al., "State of the ART report on nuclear aerosol," *Nuclerar Energy Agency Committee on The Safety of Nuclear of Nuclear Installations*, 2009.

[9] L. L. Humphries, V. G. Figueroa, M. F. Young et al., "MELCOR Computer Code Manuals Volume 1: Primer and Users' Guide," Tech. Rep. SAND2015-6691R, Sandia National Laboratories, 2015.

[10] K. Murata, D. Williams, R. Griffith et al., "Code manual for Contain 2.0: a computer code for nuclear reactor containment analysis, NUREG/CR-6533 SAND97-1735," Sandia National Laboratories, USA, 1997.

[11] P. Chatelard, S. Belon, L. Bosland et al., "Main modelling features of the ASTEC V2.1 major version," *Annals of Nuclear Energy*, vol. 93, pp. 83–93, 2016.

[12] Global Research for Safety, *COCOSYS v1.2 User'S Manual*, Berlin, Germany, 2000.

[13] M. Kajimoto, A. Hidaka, K. Muramatsu et al., *A computer code for the analysis of radionuclide transport and deposition under severe accident conditions*, Japan Atomic Energy Research Institute, Japan, 1988.

[14] A. Hidaka and J. Sugimoto, *NEA-1581 ART Mod 2*, Nuclear Energy Agency, 2015, https://www.oecd-nea.org/tools/abstract/detail/nea-1581/.

[15] A. Hidaka, K. Hashimoto, J. Sugimoto et al., "Experiment Analysis with ART Code FP Behavior under severe accident conditions, Validation of Systems Transients Analysis Codes," Tech. Rep., Japan Atomic Energy Research Institute, 1995.

[16] P. Kittiwarapon, S. Rassame, and K. Silva, "The study of cesium iodide transportation in containment of a generation III+ boiling water reactor under bypass condition," in *Proceedings of the 2015 American Nuclear Society Annual Meeting*, Los Angeles, Calif, USA, June 2015.

[17] W. Vechgama, K. Silva, and S. Rassame, "Investigation and modification of aerosol deposition model of ART Mod 2 using experimental data from NSPP-502 and Phébus FPT1," in *Proceedings of the eleventh International Topical Meeting on Nuclear Reactor Thermal-Hydraulics, Operation and Safety*, Gyeongju, Korea, October 2016.

[18] F. Souto, F. Haskin, and L. Kmetyk, "MELCOR 1.8.2 assessment: aerosol experiments ABCOVE AB5, AB6, AB7, and LACE LA2," Sandia National Laboratories, USA, 1994.

[19] G. Gyenes and L. Ammirabile, "Containment analysis on the PHEBUS FPT-0, FPT-1 and FPT-2 experiments," *Nuclear Engineering and Design*, vol. 241, no. 3, pp. 854–864, 2011.

[20] L. E. Herranz, M. Vela-García, J. Fontanet, and C. L. D. Prá, "Experimental interpretation and code validation based on the PHEBUS-FP programme: Lessons learnt from the analysis of the containment scenario of FPT1 and FPT2 tests," *Nuclear Engineering and Design*, vol. 237, no. 23, pp. 2210–2218, 2007.

[21] A. Kontautas, E. Babilas, and E. Urbonavičius, "COCOSYS analysis for deposition of aerosols and fission products in PHEBUS FPT-2 containment," *Nuclear Engineering and Design*, vol. 247, pp. 160–167, 2012.

[22] B. Clément and R. Zeyen, "The objectives of the Phébus FP experimental programme and main findings," *Annals of Nuclear Energy*, vol. 61, pp. 4–10, 2013.

[23] M. Laurie, P. March, B. Simondi-Teisseire, and F. Payot, "Reprint of "containment behaviour in Phébus FP"," *Annals of Nuclear Energy*, vol. 61, pp. 122–134, 2013.

[24] A. Nieminen, "Fission product behaviour in the containment," in *Proceedings of the Nuclear Science and Technology Symposium*

- *NST2016*, Marina Congress Center, Helsinki, Finland, 2-3 November 2016.

[25] P. March and B. Simondi-Teisseire, "Overview of the facility and experiments performed in Phébus FP," *Annals of Nuclear Energy*, vol. 61, pp. 11–22, 2013.

[26] L. E. Herranz, "Fission Product Behavior and Transport," in *Joint ICTP-IAEA 1st Course on Scientific Novelties in Phenomenology of Severe Accidents in Water Cooled Reactors (WCRs)*, ICTP-IAEA, Trieste, Italy, 2018.

[27] T. S. Kress, "Proceedings of The CSNI Specialists Meeting on Nuclear Aerosols in Reactor Safety," *U.S. Nuclear Regulatory Commission*, 1980.

[28] R. A. Serway and W. J. Jewette, *Physics for Scientists and Engineers*, Brooks/Cole, USA, 9th edition, 2014.

[29] D. D. McCoy and T. J. Hanratty, "Rate of deposition of droplets in annular two-phase flow," *International Journal of Multiphase Flow*, vol. 3, no. 4, pp. 319–331, 1977.

[30] Y. A. Cengel and J. M. Cimbala, *Fluid Mechanics Fundamentals and Applications*, McGraw-Hill, New York, NY, USA, 2006.

[31] A. Moshfegh, M. Shams, G. Ahmadi et al., "A novel slip correction factor for spherical aerosol particles," *World Academy of Science, Engineering and Technology*, vol. 27, pp. 709–715, 2009.

[32] M. F. Ashby, *Materials Selection in Mechanical Design*, Butterworth-Heinemann Ltd, London, UK, 3rd edition, 2005.

[33] L. Talbot, R. K. Cheng, R. W. Schefer et al., "Thermophoresis of particles in a heated boundary layer," *Journal of Fluid Mechanics*, vol. 101, no. 4, pp. 737–758, 1980.

[34] L. J. Siefken, E. W. Coryell, E. A. Harvego et al., *User manual of RELAP5 mod 3.3. Idaho National Engineering and Environmental Laboratory*, Idaho through the Nuclear Regulatory Commission, USA, 2000.

[35] A. Kontautas and E. Urbonavicius, "Parametric analysis of aerosol mass deposition in phebus containment under FPT-3," in *Proceedings of Nuclear Energy for New Europe*, Bled, Slovenia, September 2018.